Journal of Biomedical Optics

BiomedicalOptics.SPIEDigitalLibrary.org

Modeling of vision loss due to vitreous hemorrhage by Monte Carlo simulation

Tarek A. Al-Saeed
Sayed Y. El-Zaiat

SPIE.

Modeling of vision loss due to vitreous hemorrhage by Monte Carlo simulation

Tarek A. Al-Saeed[a,*] **and Sayed Y. El-Zaiat**[b]
[a]Helwan University, Faculty of Engineering, Biomedical Engineering Department, 1 Sherif Street, Helwan, 11792, Cairo, Egypt
[b]Ain-Shams University, Faculty of Science, Physics Department, Abbassia, 11566, Cairo, Egypt

Abstract. Vitreous hemorrhage is the leaking of blood into the vitreous humor which results from different diseases. Vitreous hemorrhage leads to vision problems ranging from mild to severe cases in which blindness occurs. Since erythrocytes are the major scatterers in blood, we are modeling light propagation in vitreous humor with erythrocytes randomly distributed in it. We consider the total medium (vitreous humor plus erythrocytes) as a turbid medium and apply Monte Carlo simulation. Then, we calculate the parameters characterizing vision loss due to vitreous hemorrhage. This work shows that the increase of the volume fraction of erythrocytes results in a decrease of the total transmittance of the vitreous body and an increase in the radius of maximum transmittance, the width of the circular strip of bright area, and the radius of the shadow area. [DOI: 10.1117/1.JBO.19.8.085009]

Keywords: eye; vision; vitreous hemorrhage; Monte Carlo.

Paper 140213RRR received Apr. 3, 2014; revised manuscript received Aug. 8, 2014; accepted for publication Aug. 8, 2014; published online Aug. 28, 2014.

1 Introduction

The vitreous humor is a clear, transparent, colorless, and jelly-like material that fills the space between the eye lens and the retina.[1] It occupies about two thirds of the volume of the eye. The vitreous humor is composed of water (∼99%), collagen, hyaluronic acid, and very few cells.[1] Further, in Ref. 1, Hea demonstrated that the refractive index of vitreous humor is ∼1.336, and in Ref. 2, Ahmed demonstrated that its volume is ∼4 ml.

In some cases, blood leaks into the vitreous humor; this is called a vitreous hemorrhage.[3–8] There are many causes of bleeding into the vitreous body, e.g., diabetic retinopathy,[9,10] retinal vein occlusion, retinal detachment, damage of retinal vessels, age-related macular degeneration,[11–14] tumors, and macroaneurysm. The symptoms of vitreous hemorrhage depend on the degree and extent of the bleeding. The symptoms include haziness of the visual field, blurry vision, shadows, red hues, appearance of spots or floaters in the vision, and, in severe cases, blindness.[9,10,15–17] A vitreous hemorrhage can be easily detected and diagnosed; e.g., at the slit lamp, erythrocytes can be seen just behind the lens by the microscope. Further, ultrasonographic examination of the eye establishes the severity and location of the hemorrhage. The echographic signs are based on blood density and blood location.[18,19]

Moreover, the blood is a highly turbid medium. It consists of 55% plasma and 45% corpuscles, 99% of which are erythrocytes and 1% of which are leukocytes and thrombocytes,[20] i.e., the optics of blood are mainly governed by plasma and erythrocytes.[21] Light scattering by erythrocytes is one of the major pathways that characterize the interaction of blood and light. In modeling erythrocytes scattering, light is considered to be an electromagnetic wave and erythrocytes are considered a dielectric body with an effective refractive index. The shape of erythrocytes may be considered as spherical or a biconcave disk or, more generally, a deformed shape.[22–25]

In the course of studying the optical effects of vitreous hemorrhage, in Ref. 21, Tuchin considered the light scattering matrix (LSM) of vitreous humor, where the light scattering matrix is a 4 by 4 matrix that connects the Stokes vector of the incident light with that of the scattered light; it describes the polarization state of the scattered light. In Ref. 21, Tuchin came to the conclusion that the vitreous humor itself does not affect the polarization of straight-transmitting light. This fact makes it possible to examine the ocular fundus and to image the optic nerve structure, which is important for the early diagnosis of glaucoma. Further, in the case of minor vitreous hemorrhage, the LSM is highly affected due to light scattering by erythrocytes.[21] Hence, in Ref. 26, Korolevich et al. considered the elements of the LSM of a monolayer of disk-shaped or spheroidal erythrocytes in relation to packing density.

In this work, for the first time to the best of our knowledge, we try to model vision loss due to vitreous hemorrhage. We assume that the vitreous humor is generally a clear and transparent medium at visible wavelengths. Moreover, erythrocytes were considered to be the predominant source of scattering in the vitreous resulting from hemorrhage. We apply Monte Carlo simulation of light propagation in the turbid medium (vitreous humor contaminated by erythrocytes).[27,28] Upon calculating the total transmittance of the vitreous body, we model the vision loss effects due to vitreous hemorrhage. Correlations between the simulated results and parameters quantifying vision loss, such as visual acuity, visual Strehl ratio (SR), and contrast sensitivity, have been discussed.

The paper is organized as follows: the first section is an introduction; the second section presents the theory of light propagation in vitreous humor and erythrocytes; the third section formulates the problem that we will solve; the fourth section

*Address all correspondence to: Tarek A. Al-Saeed, E-mail: tarek1971@ieee.org

0091-3286/2014/$25.00 © 2014 SPIE

gives the results of our simulation; the fifth section presents a discussion of the benefits of these results; and finally, the sixth section presents the conclusion and future work.

2 Theoretical Background

In this section, we give the theory of optical properties of both vitreous humor and erythrocytes.

2.1 *Refractive Index of Vitreous Humor*

In our analysis, we consider that the vitreous humor is a clear, transparent medium in the visible wavelength range, i.e., we neglect any scattering and absorption for the visible range. Thus, we are considering only the refractive index of vitreous humor which is governed by Sellmeier's equation[29]

$$n_v^2 = 1 + \frac{0.79\lambda^2}{\lambda^2 - 146^2}, \tag{1}$$

where λ is wavelength in nm and n_v is the refractive index of vitreous humor.

2.2 *Optical Properties of Erythrocytes*

The optical properties of erythrocytes depend on many factors as follows:

2.2.1 *Effective refractive index of erythrocytes*

The real part of the effective refractive index of erythrocytes varies from 1.398 to 1.404 in the wavelength range from 400 to 1000 nm and the imaginary part varies from 10^{-3} to 10^{-6} in the wavelength range from 400 to 1000 nm.[20,30]

2.2.2 *Structure of erythrocytes*

Normally, erythrocytes are shaped like a biconcave disk with an average volume of 90 μm^3, as in Refs. 20, 21, and 25. The scattering properties of erythrocytes depend on orientation, but for a large number of such particles, they can be modeled by randomly distributed spherical particles of equivalent volume.[20] Further, the volume of such particles may actually exceed the volume of normal erythrocytes due to aggregation. In our analysis, we assume no aggregation and assume a constant volume of 90 μm^3.

We employed the spherical model of erythrocytes because their optical properties can be calculated using the Mie formula. This simplification is used for several reasons. First, the methods and algorithms for calculating optical properties of aspherical scatterers are cumbersome and only have limited applicability. Second, light scattering indicatrix in the forward hemisphere for spheroids and cylinders with moderate asphericity parameters (from 0.5 to 2.0) that are averaged over different spatial orientations is the same as the indicatrix of a sphere of the same value.[31]

Moreover, the mean volume of erythrocytes is 90 μm^3 and the volume of erythrocytes in blood has a distribution function that ranges from 30 to 200 μm^3. This distribution function exhibits the presence of particles whose volume considerably exceeds the volume of a normal erythrocyte which is associated with the aggregation of erythrocytes into large-size clusters. Further, this distribution function reaches its maximum at 90 μm^3 and has a full width half maximum (FWHM) of ~25 μm^3 as in Refs. 20 and 21. Thus, for accurate analysis of the scattering of erythrocytes, especially for the case of blood, one needs to take the distribution function of the erythrocytes' volume. In the case of erythrocytes in the vitreous humor, such accuracy is not necessary since the number of erythrocytes and their density in blood is much greater than that in the vitreous humor. Therefore, our analysis will be in error to some extent if we only use an average value instead of a distribution function. Moreover, taking the volume distribution function into account is a topic that may be considered in future research.

2.2.3 *Mie theory for erythrocytes*

We apply Mie theory to erythrocytes considering them as homogeneous spheres with radius r_0. Thus, we obtain the scattering cross-section, extinction cross-section, and anisotropy factor.[22,23] The scattering cross-section is[22]

$$C_{\text{sca}} = \frac{2\pi}{k_v^2}\sum_{n=1}^{\infty}(2n+1)(|a_n|^2 + |b_n|^2). \tag{2}$$

The extinction cross-section is[22]

$$C_{\text{ext}} = \frac{2\pi}{k_v^2}\sum_{n=1}^{\infty}(2n+1)\text{Re}\{a_n + b_n\}. \tag{3}$$

The absorption cross-section is[22]

$$C_{\text{abs}} = C_{\text{ext}} - C_{\text{sca}}. \tag{4}$$

The anisotropy factor is[22]

$$g = \frac{4\pi r_0^2}{x^2 C_{\text{sca}}}\left[\sum_{n=1}^{\infty}\frac{n(n+2)}{n+1}\text{Re}\{a_n a_{n+1}^* + b_n b_{n+1}^*\} + \sum_{n=1}^{\infty}\frac{2n+1}{n(n+1)}\text{Re}\{a_n b_n^*\}\right], \tag{5}$$

where the diffraction size of the erythrocyte x is given by[22]

$$x = k_v r_0 = n_v\frac{2\pi}{\lambda}r_0, \tag{6}$$

where r_0 is the radius of the erythrocytes and n_v is the refractive index of the vitreous humor. Further, the relative refractive index of the erythrocyte m is given by

$$m = \frac{k_e}{k_v} = \frac{n_e + j\chi_e}{n_v}, \tag{7}$$

where n_e and χ_e are the real and imaginary parts of the refractive index of erythrocytes, respectively.

Finally, a_n and b_n are the Mie coefficients and the asterisk denotes the complex conjugate. The expressions of Mie coefficients are given by[22]

$$a_n = \frac{m\psi_n(mx)\psi_n'(x) - \psi_n(x)\psi_n'(mx)}{m\psi_n(mx)\xi_n'(x) - \xi_n(x)\psi_n'(mx)}, \tag{8}$$

$$b_n = \frac{\psi_n(mx)\psi_n'(x) - m\psi_n(x)\psi_n'(mx)}{\psi_n(mx)\xi_n'(x) - m\xi_n(x)\psi_n'(mx)}, \tag{9}$$

where $\psi_n(\rho) = \rho j_n(\rho)$ and $\xi_n(\rho) = \rho h_n^{(1)}(\rho)$ are the Reccati-Bessel functions, $j_n(\rho)$ is the spherical Bessel function of the first kind of order n, and $h_n^{(1)}(\rho)$ is the spherical Bessel function of the third kind of order n (sometimes called the spherical Hankel function of the first kind).

2.2.4 *Scattering and absorption coefficients of erythrocytes*

The scattering coefficient of erythrocytes is given by[22]

$$\mu_s = N_e C_{\text{sca}}, \tag{10}$$

where N_e is the number of erythrocytes per unit volume, which is given by

$$N_e = \frac{3}{4\pi r_0^3}\eta, \tag{11}$$

where η is the volume fraction of erythrocytes. Similarly, the absorption coefficient is given by[22]

$$\mu_a = N_e C_{\text{abs}}. \tag{12}$$

2.2.5 *Phase function*

The phase function is the probability density function of the cosine of the scattering angle. The Mie theoretical phase function is more useful and accurate than any other phase function. However, the Henyey-Greenstein (HG) phase function is a good approximation of a phase function and is simple to use. It is given by[32]

$$p_{\text{HG}}(\cos\,\theta) = \frac{1-g^2}{2(1+g^2-2\,g\cos\,\theta)^{3/2}}, \tag{13}$$

where g is the anisotropy factor, which represents the average of the cosine of the scattering angel θ, which ranges from -1 to 1.

It should be noted that Mie theory rigorously describes the scattering of light by a sphere. It is an exact solution of Maxwell's electromagnetic field equations for a homogeneous sphere, which is the case of the erythrocytes considered in our simulation. For some calculations, the theoretical Mie phase function may be useful. On the other hand, the HG phase function is an approximation to that of Mie. It is widely employed in radiative transport calculations for the description of the scattering process in blood because of their mathematical simplicity. However, the HG phase function cannot be used for accurate calculations of the angular light distribution scattered by a single erythrocyte.[21]

3 Problem Modeling

In our study of light propagation in the vitreous body, we assume no scattering or absorption in the vitreous humor. The unique source of scattering and absorption is the leaked erythrocytes. Thus, we treat the vitreous humor contaminated by erythrocytes as a turbid medium. The absorption coefficient, the scattering coefficient, and the anisotropy factor are that of spherical erythrocytes calculated by Mie theory in the previous section. The phase function is that of HG.[32] Thus, we apply Monte Carlo simulation of light propagation in the vitreous humor contaminated by erythrocytes.

In our analysis of the vitreous body, we assume that we have a layer of clear vitreous humor. This layer has a thickness of 16 mm and it has infinite extents in the other two directions. This should not be considered contradictory with the physical shape of the vitreous body which is nearly spherical, because here we model only the introduction of erythrocytes in the vitreous humor. Afterward, we vary the amounts of erythrocytes. To quantify the amounts of erythrocytes we use the volume fraction, which is the ratio of the total volume occupied by erythrocytes to the volume of the vitreous humor.

In applying Monte Carlo simulation,[27,28] we assume we have a pencil beam perpendicularly incident on the layer of vitreous humor, i.e., we obtain the impulse response. Further, we assume we have a matched layer, i.e., we assume the surrounding medium has the same refractive index. This is not strange because we are only interested in the scattering and absorption effects of erythrocytes in the vitreous humor. Finally, we are interested in calculating the transmittance of that layer under varying concentrations of erythrocytes in the vitreous humor.

In the following section, we present the numerical values of Monte Carlo simulation.

4 Simulation Results

In this section, we introduce the numerical values obtained in our simulation. First, the working wavelength is 600 nm. We obtain the refractive indices of vitreous humor and erythrocytes n_v and $n_e + j\chi_e$, respectively, as in Sec. 2. Then, we obtain μ_s, μ_a, and g from Mie theory. We apply Monte Carlo simulation[27,28] to the layer of vitreous humor as shown in Fig. 1.

In our simulation, we have two different cases of erythrocytes distribution. In the first case, we assume that we have

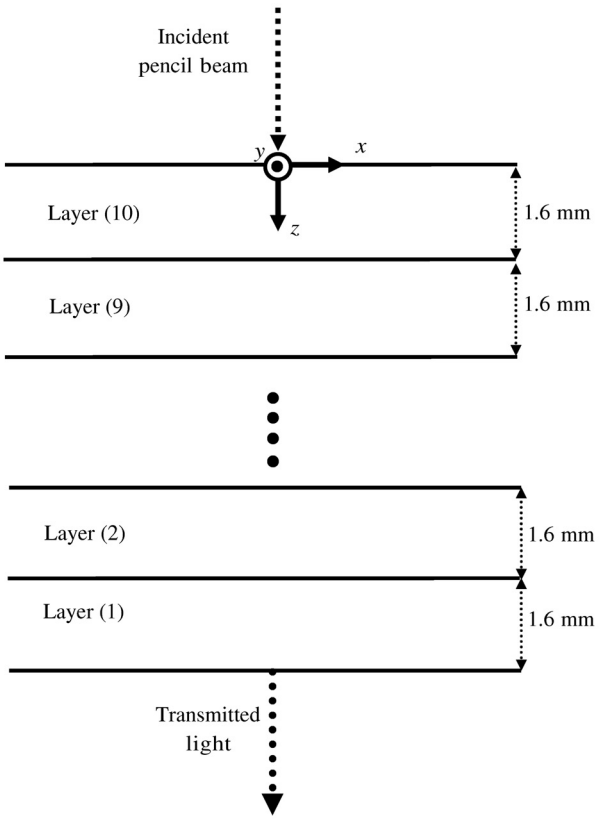

Fig. 1 Schematic diagram of the problem.

uniform distribution with a constant concentration of erythrocytes throughout the whole vitreous body, whose thickness is 16 mm. In the second case, we assume an exponentially varying distribution of erythrocytes whose concentration decreases exponentially, i.e., exponentially decreasing as we go away from the retina. To account for a varying distribution, we divide the whole vitreous layer into 10 layers, as in Fig. 1. Each layer has a constant concentration. Each layer concentration exponentially decreases compared to the first layer.

Further, in our Monte Carlo simulation, we used 2×10^5 photons. Thus, the obtained numerical values of transmittance are stable for at least the two most significant digits, i.e., using more photons will not change the obtained values up to more than the first most significant digit. This stability of numerical values is highly sufficient for our modeling purposes. Moreover, the discretization step in the radial dimension is 100 μm. This value is not so great to be coarse and not so small so that, for the above-mentioned number of photons, we do not have high fluctuations. Thus, the resolution used in calculating various radius-based quantities is 100 μm, which is acceptable for our modeling purposes.

4.1 *Results of Uniform Concentration*

We apply Monte Carlo simulation for a single matched layer of vitreous humor of 16 mm thickness, which has a uniform concentration of erythrocytes characterized by a volume fraction. Then we calculate the transmittance of this layer. The layer has cylindrical symmetry, thus we calculate transmittance as a function of the radial coordinate r defined as

$$r = \sqrt{x^2 + y^2}, \tag{14}$$

where x and y are the Cartesian coordinates as shown in Fig. 1. We calculate the total transmittance as function of r and plot Fig. 2 in which we have a family of curves presenting three different volume fractions of erythrocytes 0.1, 0.5, and 1%. In each curve, we should distinguish the following parameters:

1. The radius of maximum transmittance, i.e., the radius at which the transmittance is maximum: this parameter accounts for the shift in position of the pencil beam as it reaches the retina.

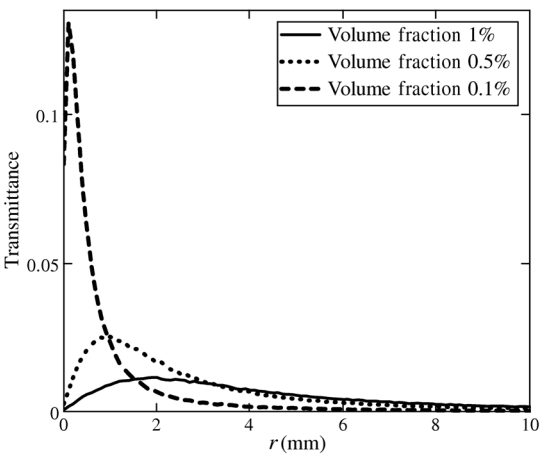

Fig. 2 Transmittance as a function of r for three different volume fractions.

2. The FWHM of the transmittance curve: this parameter accounts for the spread of the pencil beam. Further, it accounts for the fact that, under vitreous hemorrhage, the pencil beam will be viewed as a circular strip of varying thickness based on volume fraction.

3. The shadow radius: this is the radial distance from $r = 0$ to r where the first half of maximum transmittance occurs. This parameter accounts for a circular disk where the patient will see a dark region. So I call it a shadow area because without erythrocytes this area should appear bright.

From Fig. 2, it is clear that the transmittance has a peak that shifts from $r = 0$. Moreover, transmittance decreases and becomes negligible at large values of r. The rate of decrease depends on the volume fraction of erythrocytes.

Further, to make these parameters clearer, we present Fig. 3. In this figure, we give a two-dimensional (2-D) plot of the transmittance for three different cases of volume fractions.

It should be noted that the shadow area results from the scattering of light by erythrocytes, which attenuates direct rays of light. To prove that this shadow area is governed by Mie scattering theory, we repeated analysis by using different values of the radius of erythrocytes, specifically 2, 2.5, 3, and 3.5 μm, and retained the same number of erythrocytes per unit volume, specifically 5.556×10^4 mm^{-3}. This last number corresponds to a volume fraction of 0.5% in the case in which the volume of a single erythrocyte is 90 μm^3. The results obtained are given in Table 1, which shows an increase of the shadow radius as the radius of erythrocytes increases. The central shadow area contributes to black spots, opacity, and shadowing due to floaters and visual field occlusion. This is what the patient can actually see. From our model, the turbid layer of the vitreous has a scattering coefficient whose effect is to impede the direct beam from being transmitted, i.e., it is the consequence of scattering by erythrocytes.

From Fig. 3(a), where the volume fraction is 1%, it is clear that the radius of maximum transmittance is the greatest and the light will spread over a large thickness circular strip. Further, the shadow area characterized by the dark area at the center of the figure has the greatest radius. In Fig. 3(c), where volume fraction is 0.1%, all of these parameters are the smallest, i.e., the pencil beam, in this case, will be viewed as a small circular strip and there will be no shadow at all. Figure 3(b), where volume fraction is 0.5%, will have values in between.

It should be noted that in Fig. 3(c), the central region actually appears darker than the surrounding regions, which means that transmittance is smaller at the center. But we do not consider it shadow because transmittance at the center is greater than the half of the maximum transmittance. We have used a threshold of half the maximum to judge whether it is a shadow or not.

To quantify the effect erythrocytes have on the above-mentioned parameters, we introduce Fig. 4. We plot the total transmittance and the previously mentioned three parameters as a function of the volume fraction of erythrocytes.

It is clear from this figure how the total transmittance and the three parameters deteriorate as the volume fraction of erythrocytes increases.

4.2 *Results of Exponentially Decreasing Concentration*

In the previous subsection, we assumed we have a uniform concentration of erythrocytes throughout the volume of the vitreous

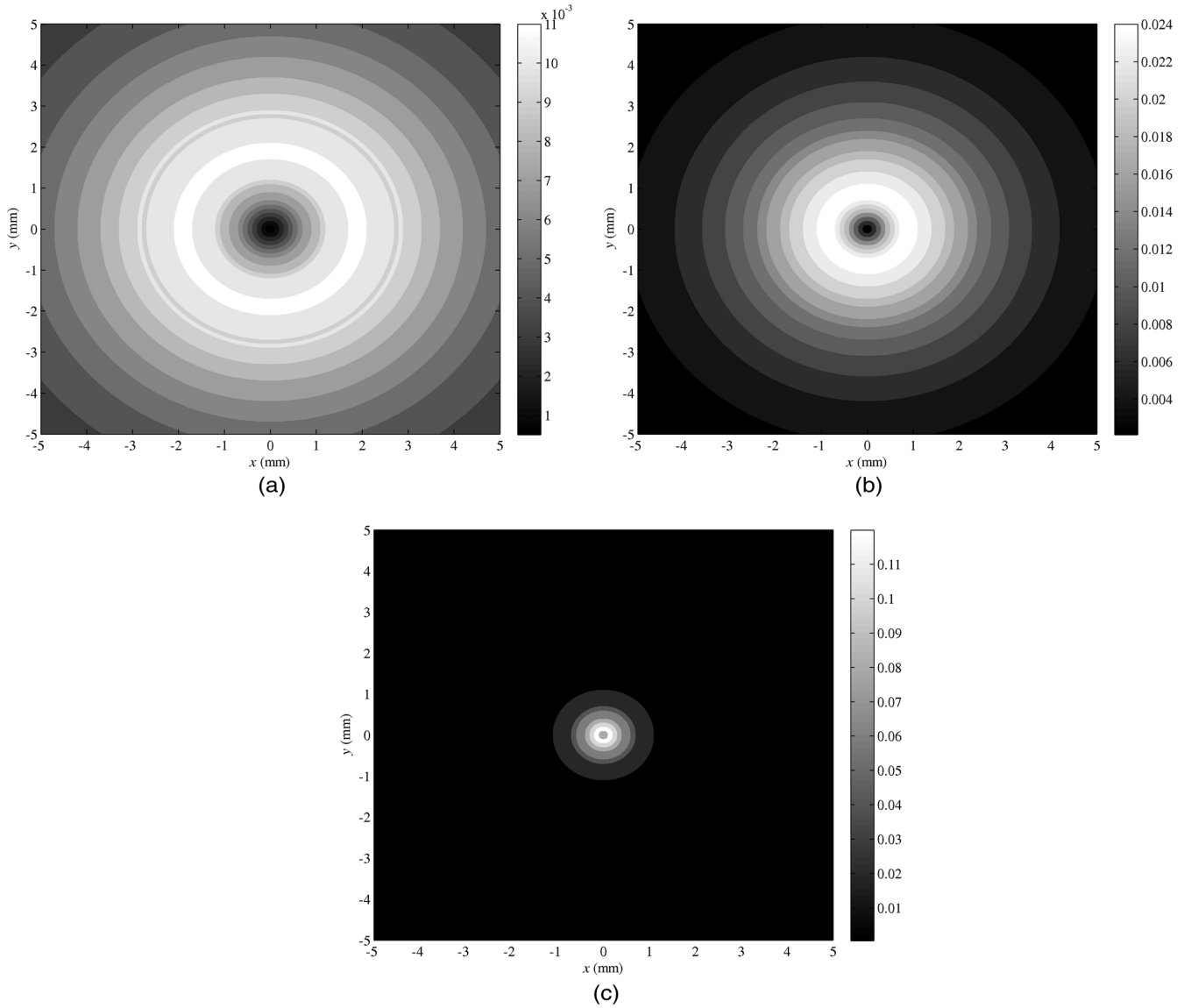

Fig. 3 Two-dimensional plot of transmittance: (a) volume fraction 1%, (b) volume fraction 0.5%, and (c) volume fraction 0.1%.

body. This assumption may appear far from reality because, in fact, erythrocytes will have a high concentration near the retina and a small concentration at the other end of the vitreous body. Thus, to account for varying erythrocytes' concentration, we divide the whole vitreous layer into 10 layers, each of which has a constant concentration that exponentially decreases. In terms of the volume fraction, each layer will have an erythrocytes volume fraction η_i in percentage, which is given by

$$\eta_i = \eta_0 \exp(-i/\sigma), \tag{15}$$

where η_0 is the volume fraction at the first layer immediately adjacent to the retina and η_i is the volume fraction at the $(i+1)$'th layer. Further, i varies from 0 to 9 and σ determines the rate with which the volume fraction decreases. It determines the layer at which the volume fraction decrease to e^{-1} of that of the first layer.

To identify the effect of exponentially decreasing concentration, we discuss two cases. In the first case, we assume a constant $\eta_0 = 5\%$ and vary σ from 1 to 9. Thus, we plot the total transmittance and the other three parameters as a function of σ in Fig. 5. In the second case, we assume constant $\sigma = 4$, i.e., the concentration decreases to e^{-1} of that of the first layer at the fifth layer. Then, we vary η_0 from 1 to 5% and plot the same four quantities as in Fig. 6.

Table 1 Parameters obtained for the case of varying erythrocytes radius.

Erythrocyte radius (μm)	Shadow radius (mm)	Radius of maximum transmittance (mm)	Full width half maximum (mm)
2	0.065	0.3	1.09
2.5	0.16	0.8	1.94
3	0.291	1	2.739
3.5	0.43	1.6	3.729

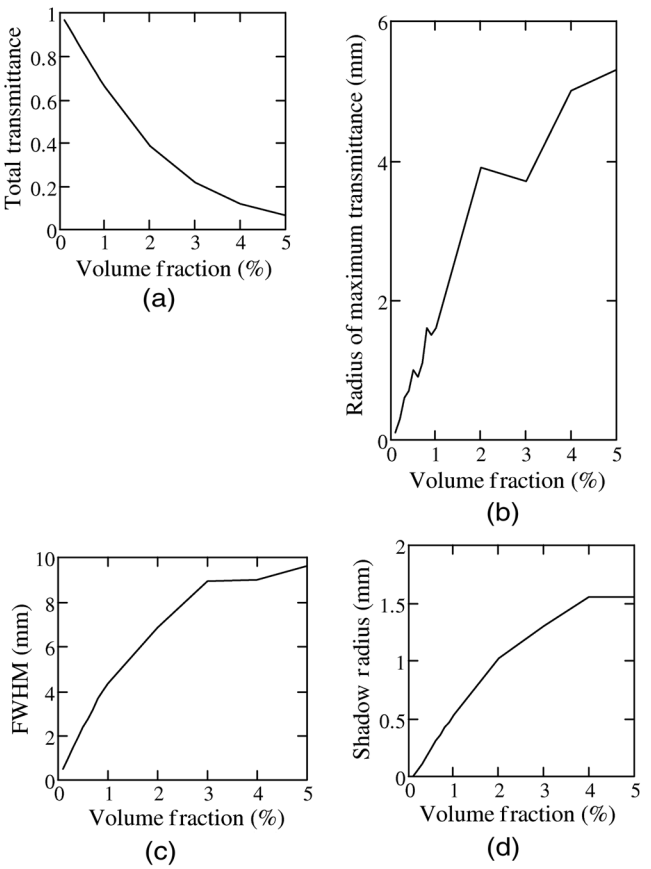

Fig. 4 The four parameters as a function of volume fraction for uniform erythrocyte concentration: (a) total transmittance, (b) radius of maximum transmittance, (c) FWHM, and (d) shadow radius.

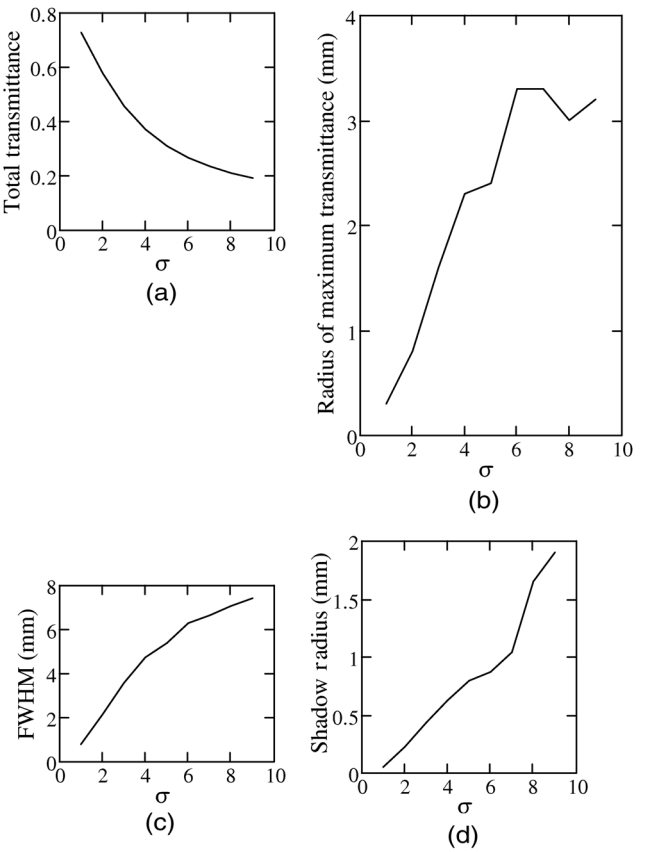

Fig. 5 The four parameters as a function of σ for an exponentially varying concentration: (a) total transmittance, (b) radius of maximum transmittance, (c) FWHM, and (d) shadow radius.

Figures 5 and 6 along with Fig. 4 ensure that the increase in the volume fraction of erythrocytes results in the following: (1) decrease in the total transmittance, (2) increase in the radius of the maximum transmittance, (3) increase in the width of the circular strip of the bright area, and (4) increase in the radius of the shadow area.

4.3 *Results of Transmittance of Gaussian Beam*

In the previous two sections, we considered a pencil beam. Although the results of a pencil beam are valuable, actual beams have finite dimensions. So in this subsection, we consider the transmittance of a Gaussian beam. Then we present the parameters of the laser beam used in the treatment of retinal diseases in the case of a vitreous hemorrhage.

4.3.1 *Analysis of Gaussian beam transmittance*

One of most common beams is the Gaussian beam whose intensity distribution is given by[33]

$$S(r) = \frac{2}{\pi W^2}\exp[-2(r/W)^2], \tag{16}$$

where $S(r)$ is the intensity, i.e., power per unit area and we assume a beam of total power of unity. We ignored divergence of the beam and specify that W is the beam radius. The obtained results of transmittance versus the radial dimension for a pencil beam in Fig. 2 can be considered as the impulse response for transmittance, which we call $G_T(r)$ and denote as the Green's function for transmittance. In order to obtain the transmittance response to a Gaussian beam, we only convolve the Green function, $G_T(r)$, with the source intensity profile $S(r)$. First, the convolution in Cartesian coordinates is given by[33]

$$T(x,y) = \int_{-\infty}^{\infty}\int_{-\infty}^{\infty} G_T(x-x_0, y-y_0)S(x_0,y_0)\mathrm{d}x_0\mathrm{d}y_0, \tag{17}$$

which can be equivalently written as[33]

$$T(x,y) = \int_{-\infty}^{\infty}\int_{-\infty}^{\infty} G_T(x_0,y_0)S(x-x_0, y-y_0)\mathrm{d}x_0\mathrm{d}y_0. \tag{18}$$

Since we have radial symmetry of both the source and Green function, the last equation can be written in polar coordinates as[33]

$$T(r) = \int_0^{2\pi}\int_{-\infty}^{\infty} G_T(\rho)S\left(\sqrt{r^2+\rho^2-2r\rho\cos\phi}\right)\rho\mathrm{d}\rho\mathrm{d}\phi. \tag{19}$$

In Fig. 7, we study the transmittance profile for Gaussian laser beams of different radii, i.e., $W = 1500$, 1000, 500, and 200 μm. In Figs. 7(a) and 7(b), we used a vitreous layer of

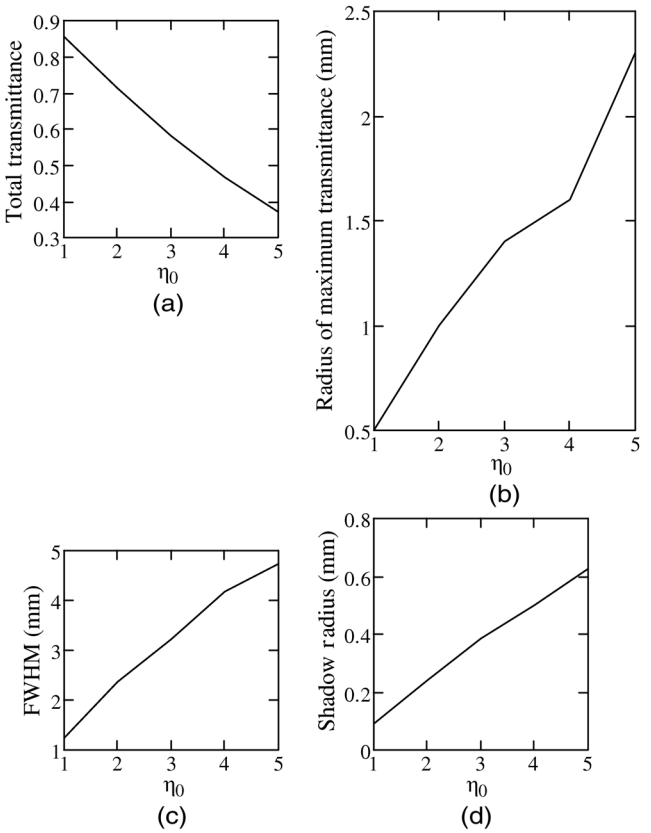

Fig. 6 The four parameters as a function of η_0 for an exponentially varying concentration: (a) total transmittance, (b) radius of maximum transmittance, (c) FWHM, and (d) shadow radius.

uniform distribution of volume concentration 1 and 0.5%, respectively.

From Fig. 7, we find out the following:

1. At large radius r, the curves of the pencil beam and Gaussian beam coincide since the Green function and the source intensity decrease with the radius r.
2. At $r = 0$ and the adjacent area, there is a great difference between the pencil beam and Gaussian beams. In the pencil beam, there is a small transmittance at $r = 0$, which is due to scattering. On the contrary, Gaussian beams have more transmittance at this position. This is because if we consider that the Gaussian beam is composed of a very large number of pencil beams distributed along the beam cross-section, each beam will be scattered into the region $r = 0$.
3. As the Gaussian beam radius decreases, we approach the pencil beam. This is clear in Fig. 7 for the case of a Gaussian beam of radius 200 μm.
4. All curves show that light is distributed over a large area, i.e., the FWHM shows values greater than the radius of the Gaussian beam. It is not limited to the case of pencil beam. Thus, any light beam, upon exiting from the vitreous body, will suffer an evitable distribution over a large area.

4.3.2 *Therapeutic laser parameters under vitreous hemorrhage*

Laser energy is used in the treatment of many retinal diseases, e.g., laser photocoagulation treatment of serous retinal detachment.[34] The parameters of the treatment are power, spot size, and time of exposure. Although laser therapy in the presence of a vitreous hemorrhage may be contraindicated in most medical circumstances, a calculation has been performed to project the operational parameters required to achieve delivery of a therapeutic dose of laser energy to the retina. These parameters are drastically different than the typical therapeutic dose suggested for treatment conditions without hemorrhage. Therefore, we consider a sample case of treatment whose parameters are[34] 100 mW power, 100 μm spot size radius, and 0.2 s exposure time.

For this case, we repeat the analysis in the previous subsection, but we use $W = 100$ μm in Eq. (16). Thus, we get curves similar to that in Fig. 7. From these curves, we get the half maximum transmittance T_{half} and consider it the average

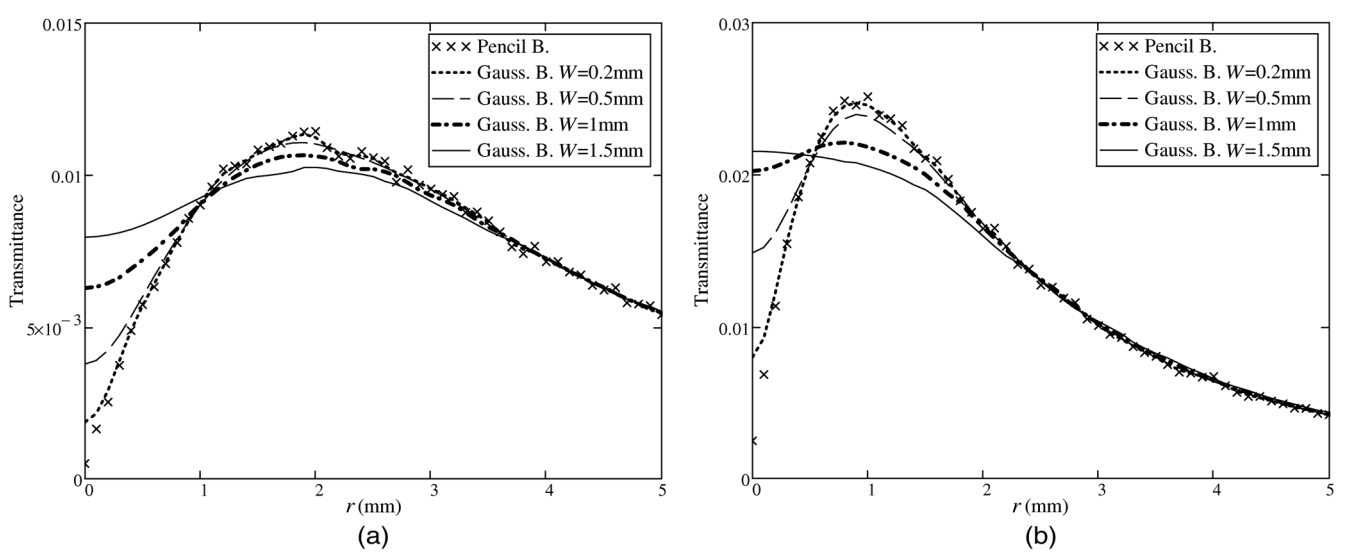

Fig. 7 Transmittance profile of Gaussian beams of different radii and a pencil beam. (a) Volume concentration of erythrocytes is 1%. (b) Volume concentration of erythrocytes is 0.5%.

transmittance. We define the energy density to be the energy delivered to the retina per unit area in J/cm^2. Energy density can be calculated by

$$E_0 = t_0 P_0, \tag{20}$$

where t_0 is the exposure time in seconds. Further, P_0 is the power density in W/cm^2 and is defined as power per unit area. This is for the case without hemorrhage. In the case of hemorrhage, we have new time t_1 and power density P_1. In our analysis, we consider the same energy per unit area delivered to the retina. Thus, setting t_1 to some reasonable value and having the same energy density in Eq. (20), we get P_1. To get the required power to be applied at the starting point of the vitreous body, i.e., at $z = 0$, we have

$$\text{Input power} = \frac{P_1}{T_{\text{half}}}. \tag{21}$$

The obtained values of power and other parameters are given in Table 2.

Note that in the previous table, the input beam is Gaussian with a spot size radius = 100 μm in all cases. Further, the exposure area in the case without hemorrhage is the area of a circle with a radius of 100 μm. In the cases with a hemorrhage, the exposure area is the area of annulus where the transmittance is greater than or equal to T_{half}.

Table 2 Sample of laser power required for retinal treatment with vitreous hemorrhage.

Volume fraction	Exposure time (s)	Exposure area (cm^2)	Input power (W)
0% (without hemorrhage)	0.2	3.142×10^{-4}	0.1
0.1%	2.0	7.39×10^{-3}	504.0
0.5%	2.0	0.228	2.564×10^{3}
1%	2.0	0.73	5.581×10^{3}

From the table, it is clear that the required power in the case of hemorrhage is tremendously greater than that in the case without hemorrhage. This is because (1) much power is absorbed by erythrocytes and (2) the laser energy is spread over a wide exposure area. For example, the ratio of the exposure area in the case of a volume fraction 1% equals ~2300 times that without a hemorrhage.

Further, it should be stressed that vitreous hemorrhage is one of the contradictions to retinal laser treatment.

4.4 *Results of Absorption*

In the previous subsections, we considered transmittance of the vitreous body. In this subsection, we consider the light absorbed in the vitreous due to erythrocytes.

First, we consider absorption in the case of an incident pencil beam. In Fig. 8(a), we calculated the total absorption in the vitreous in the case of a uniform distribution of erythrocytes with a varying volume fraction. It is clear that absorption increases as the volume fraction increases.

Further, to get some parameter that characterizes absorption and since the total medium examined has infinite radial dimension, we consider the absorption in horizontal layers, which for each depth z, is the sum of absorption across the radius r. Thus, we define the layer absorption as

$$\text{Horizontal layer absorption}(z) = \sum_r \text{Absorption}(r, z), \tag{22}$$

where $\text{Absorption}(r, z)$ is the absorption distribution in radial dimension r and depth z. In Fig. 8(b), we plot the horizontal layer absorption as a function of depth z for different uniform distributions of volume fractions 5, 3, and 1%. It is clear from this figure that absorption decreases with depth and has a position where the absorption has a maximum value. Thus, we consider a parameter, which is the depth of the layer of maximum absorption, and plot it in Fig. 8(c) for varying uniform

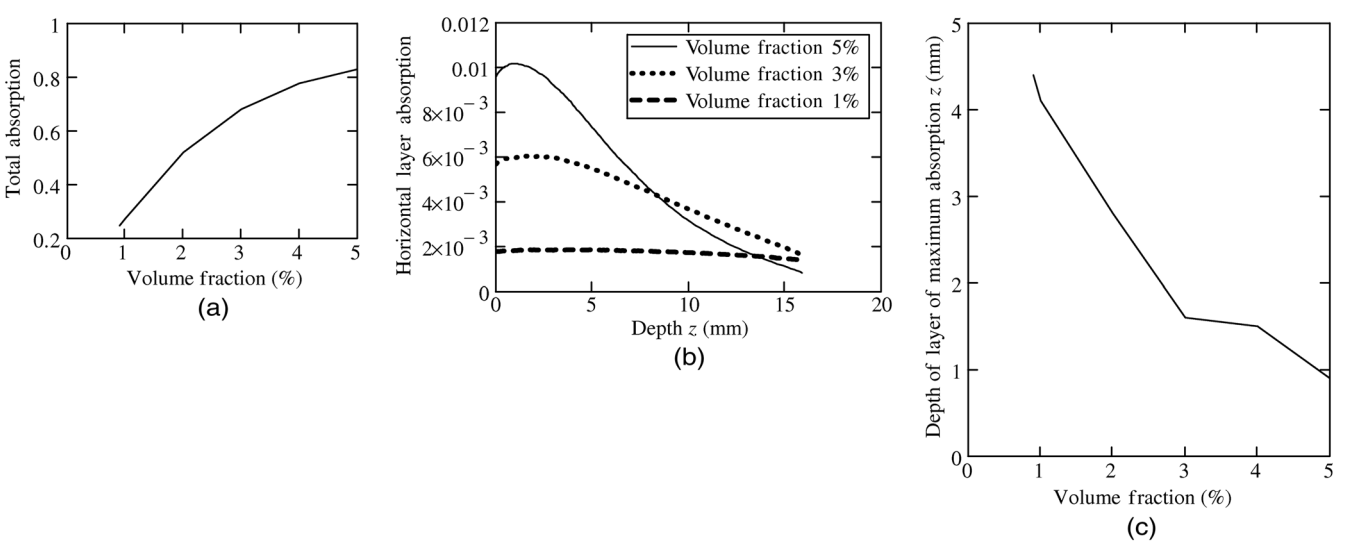

Fig. 8 Absorption parameters: (a) total absorption versus volume fraction, (b) horizontal layer absorption as a function of depth *z*, and (c) depth of layer of maximum absorption as a function of volume fraction.

distributions. It is clear that for a large volume fraction, the absorption peak is near the surface of the vitreous and for a low volume fraction, the absorption peak goes deeply into the vitreous. This is true because at a high volume fraction, absorption and scattering coefficients are greater. Therefore, photons do not have chance to travel deep in the vitreous because of large scattering and absorption.

Second, we consider absorption due to incident Gaussian beams of different radii. The obtained distribution of absorption for a pencil beam, in the first part of this subsection, can be considered as the Green's function for absorption $G_A(r,z)$. Therefore, to obtain the absorption for a Gaussian beam, we use the convolution Eq. (19) for absorption instead of transmission.[33]

$$A(r,z)=\int_0^{2\pi}\int_{-\infty}^{\infty} G_A(\rho,z)S(\sqrt{r^2+\rho^2-2r\rho\cos\phi})\rho\mathrm{d}\rho\mathrm{d}\phi, \tag{23}$$

where $A(r,z)$ is the absorption distribution for a Gaussian beam. In Fig. 9, we plot the absorption distribution in r and z, for pencil beams and Gaussian beams of radii 1500, 1000, and 500 μm. In this figure, we used a uniform distribution of erythrocytes with a volume fraction of 5%. Further, the values of absorption are normalized to the maximum and multiplied by 100 to get the percent values of the maximum.

For the case of a pencil beam, absorption is confined to the point of incidence $r=0$ and $z=0$. In Gaussian beams, absorption has a maximum point which is located deeper in the z direction. Further, in Gaussian beams, absorption is more distributed in the radial dimension. This distribution is due to the fact that the source spreads over a large area where the Gaussian beam can be considered to be composed of a large number of pencil beams distributed in the radial dimension. Further, the nonuniform distribution of absorption may result in changing the physical properties due to heating, especially at positions of peak absorption.[35]

4.5 *Prediction of Loss in Visual Performance*

In this subsection, we make a correlation between the obtained results and the parameters quantifying vision loss. We discuss visual acuity, visual SR, and contrast sensitivity.

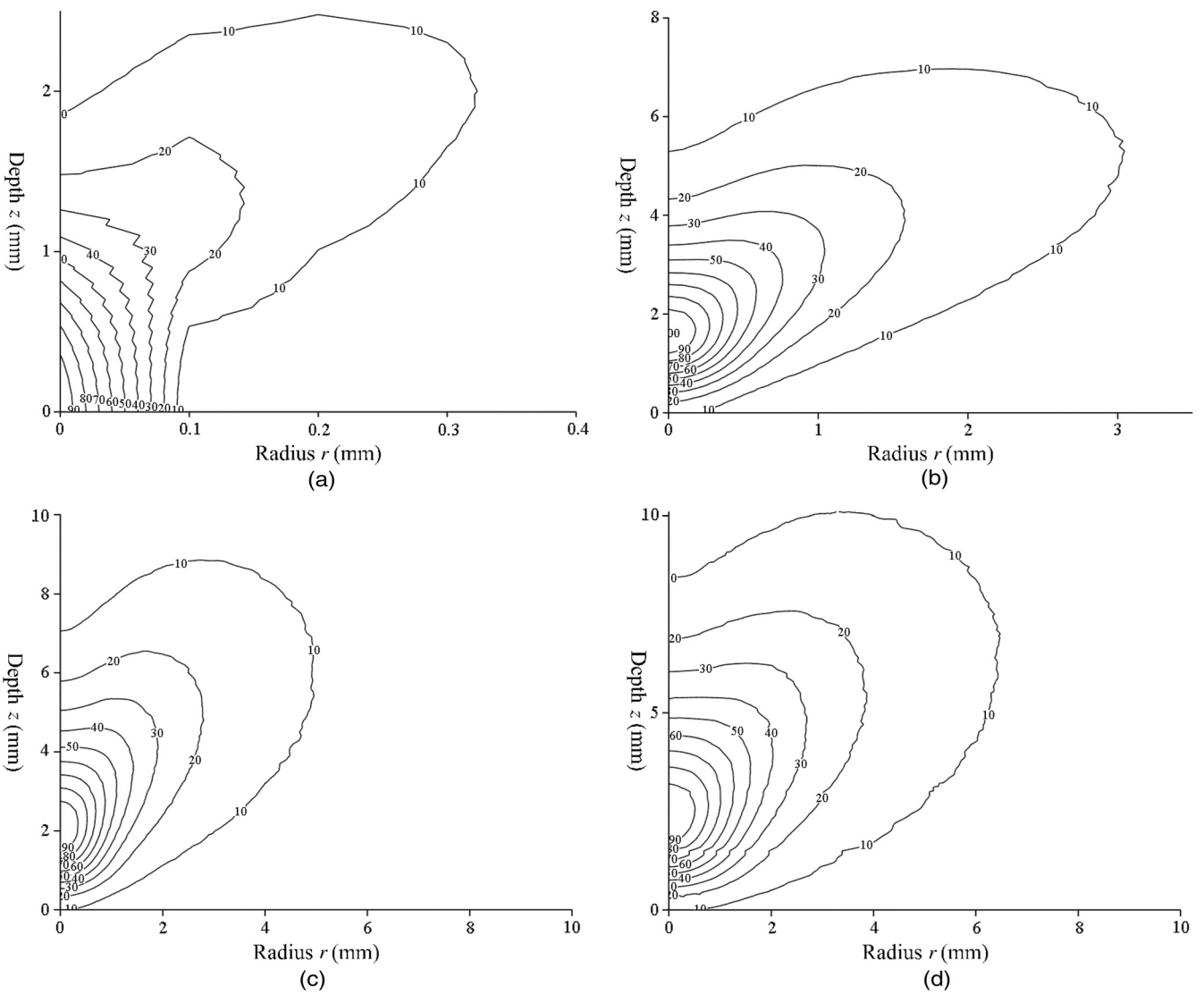

Fig. 9 Absorption distribution: (a) pencil beam, (b) Gaussian beam of radius 500 μm, (c) Gaussian beam of radius 1000 μm, and (d) Gaussian beam of radius 1500 μm.

4.5.1 *Visual acuity*

Visual acuity is the main parameter used for the ophthalmologist to evaluate the performance of the visual system. The most common method to test visual acuity is to use the standard Snellen chart.[36] The minimum size of the targets (optotypes) for which the number of correct answers is above the threshold determines the value of visual acuity.[36]

Visual acuity was derived from the maximum spatial resolution of the human eye. This resolution can be obtained from the modulation transfer function (MTF). This function can be obtained from the normalized modulus of the 2-D Fourier transform of the response in Fig. 3. Thus, in Fig. 10, we obtained the MTF for three different cases of concentration: 0.1, 0.5, and 1%. This function works as a low-pass filter with the frequency response decreasing as we increase the volume fraction of erythrocytes.

In the Snellen chart used, the optotype is a letter E and the patient stands 20 ft from the chart.[36] Further, at spatial frequency f (cycle/degree), the minimum intersection angle identified by human eye is $1/f$. Correspondingly, the height of the minimum size letter identified by the human eye is $2.5 \times 20 \times (1/f)$. Here, the number of 20 indicates the distance of 20 ft from the chart where the individual stands to read the letters, and 2.5 is the cycle of the letter E.[36] The distance of the minimum size letter height of $2.5 \times 20 \times (1/f)$ forming a 5 min angle (5/60 deg) is L

$$L = \frac{2.5 \times 20}{f \times (5/60)}. \tag{24}$$

Thus, visual acuity is[36]

$$\text{Visual acuity} = \frac{20}{L} = \frac{f}{30}. \tag{25}$$

In Fig. 10, we draw vertical dash-dotted lines to mark the spatial frequencies of different acuity values. A degradation in visual acuity is clear as the concentration of erythrocytes increases.

4.5.2 *Visual Strehl ratio*

SR is frequently defined as the ratio of the peak aberrated image intensity from a point source compared to the maximum attainable intensity using an ideal optical system limited only by diffraction over the system's aperture.[37] It is also often expressed in terms not of the peak intensity but of the intensity at the image center (intersection of the optical axis with the focal plane) due to an on-axis source; in most important cases, these definitions result in a very similar figure.

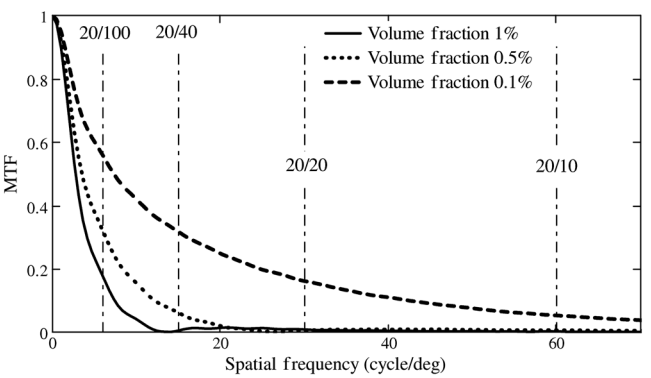

Fig. 10 Modulation transfer function versus spatial frequency for different volume fractions. Visual acuity values are marked at corresponding frequencies.

Since, in our analysis, we are not considering lenses, we limit the definition of SR to the ratio of the peak transmittance from the vitreous body with erythrocytes to the peak of transmittance, which is limited only by diffraction, i.e., in the vitreous without erythrocytes.

To account for the case that is limited only by diffraction, we use the Gaussian beam used in Sec. 4.3.1. The waist of the Gaussian beam is located at $z = 0$. So, as this beam propagates through the vitreous body, its radius increases. Thus, this Gaussian beam can be used to account for diffraction effects. In the case of vitreous without erythrocytes, the maximum transmittance will be

$$T_{\text{without}} = \frac{2}{\pi W_{z=d}^2}, \tag{26}$$

where $W_{z=d}$ is the beam radius at $z = d$, which is related to that at $z = 0$ by[38]

$$W_{z=d}^2 = W^2 \left[1 + \left(\frac{\lambda d}{n_v \pi W^2}\right)^2\right], \tag{27}$$

where W is the beam radius at $z = 0$, $d = 1.6$ cm is the vitreous layer thickness, n_v is the refractive index of the vitreous, and $\lambda = 600$ nm is the wavelength.

Thus, SR will be the ratio of maxima in Fig. 7 to T_{without}.

It is clear from Table 3 that the values of SR are small; this is because of attenuation due to absorption in erythrocytes and the spreading due to scattering by erythrocytes.

4.5.3 *Contrast sensitivity*

Contrast is the difference in luminance and/or color that makes an object (or its representation in an image or display) distinguishable.[39] Suppose we present a visual target on a uniform background. The contrast of the target quantifies its relative difference in luminance from the background and may be specified as the Weber contrast[39]

$$\text{Contrast} = \frac{I_{\max} - I_{\min}}{I_{\text{background}}}, \tag{28}$$

Table 3 Visual Strehl ratio for Gaussian beams with different spot sizes.

Volume fraction	Strehl ratio			
	$W = 200\ \mu$m	$W = 500\ \mu$m	$W = 1000\ \mu$m	$W = 1500\ \mu$m
0.1%	7.757×10^{-5}	3.731×10^{-4}	9.0×10^{-4}	1.356×10^{-3}
0.5%	1.557×10^{-5}	9.405×10^{-5}	3.471×10^{-4}	7.605×10^{-4}
1%	7.142×10^{-6}	4.344×10^{-5}	1.672×10^{-4}	3.62×10^{-4}

where I_{max}, I_{min}, and $I_{background}$ are luminance maximum, minimum, and background, respectively. Further, in our model, we have a pencil beam of light surrounded by a black background. If we considered that the background luminance is very small, then the detected intensity with and without vitreous hemorrhage will be nearly the same. On the contrary, the maximum luminance will be degraded for the best case by T_{max}, where T_{max} is the maximum of transmittance obtained in the curves of Fig. 2. So, the contrast with vitreous hemorrhage is related to that without vitreous hemorrhage by

$$\begin{aligned}&\text{Contrast with hemorrhage}\\&= T_{max}(\text{Contrast without hemorrhage})\\&= T_{max}\frac{I_{max}-I_{min}}{I_{background}}.\end{aligned} \tag{29}$$

Note that T_{max} is always <1.

Contrast sensitivity defines the threshold between the visible and invisible. It is reported in Ref. 39 that threshold contrast is 1% for a remarkably wide range of targets and conditions. Thus, in the case of hemorrhage, this threshold will be $(1/T_{max})\%$, which means contrast sensitivity will be degraded by the inverse of the maximum value of transmittance.

5 Discussion

To the best of our knowledge, this is the first time light propagation in the vitreous humor with various concentrations of erythrocytes as a tool of modeling optical properties and effects of vitreous hemorrhage has been discussed. Previous work examined only the effects of erythrocytes on a light scattering matrix.[26]

We studied the effects of varying erythrocytes' concentration on transmittance, which is an important parameter to measure the degree of partial vision loss due to a vitreous hemorrhage. This is done by considering the volume fraction occupied by erythrocytes, which is the parameter that characterizes the existence of erythrocytes.

We applied calculations to two different cases. The first is the uniform distribution of erythrocytes, and the second case is the exponentially decreasing concentration. Although the latter case appears to be more physical, the former is important in showing the extent to which the concentration of erythrocytes affects transmittance.

In one case of exponentially decreasing concentration, we made the concentration in the first layer equal to the worst case concentration considered in the uniform concentration case. Further, in another case, we made the first layer concentration (i.e., volume fraction) vary from 1 to 5% with a constant rate of exponential decrease in the other layers. This is done for the sake of simulating the actual distribution of erythrocytes into the vitreous humor.

We also provided a 2-D plot of the transmittance as a function of the radial dimension centered on the incident pencil beam. In these plots, it should be stressed that plots with large bright region means that light from the pencil beam is very broadened. On the contrary, plots with a very narrow bright region means that the pencil beam suffers the least amount of broadening.

The obtained parameters are important because they account for degradation of the visual function as follows:

1. Total transmittance of the vitreous body accounts for the loss of brightness of the imaged scene.
2. Shadow radius contributes to black spots, opacity, and shadowing due to floaters.
3. FWHM accounts for loss of resolution.
4. Radius of maximum transmittance accounts for deviation of light rays from their direct path, which, in turn, is a source of distortion of the scene.

Ultrasonographic examination of the eye is essential for establishing the severity of hemorrhage and can be useful when deciding between early surgery or waiting for spontaneous clearing. On the other hand, our model is important for predicting the severity of the hemorrhage.

The parameter FWHM (thickness of the region of full width half maximum of transmittance), which accounts for loss of vision resolution (disability to discriminate fine details of the scene), is useful for predicting the severity of the hemorrhage. We suggest a test to check the ability of the patient to discriminate minute details. For example, the clinician can give the patient a board on which English letters are written with ascending sizes and ask him to read the letters. If the patient can read very small letters, then the case is not dangerous and does not need surgery. If the patient cannot read very small letters but reads larger letters, this may be a check to differentiate between moderate, mild, and severe cases. This test may be used in parallel with a B-scan.

Further, the effect of the obtained parameters can be extended to the treatment. If the clinician decided to use a laser to fix the cause of the vitreous hemorrhage, e.g., closing retinal tears, these quantities reflect the problem the patient will suffer. First, the total transmittance of the vitreous in this case will reflect how much power of the laser beam reaches the retina. Thus, very small values of transmission mean that laser power is not sufficient for photocoagulation, for example. Second, FWHM reflects the distribution of the laser beam; thus, the intensity of the laser beam may not be sufficient for treatment. Moreover, for a very small radius of Gaussian beam (e.g., 200 μm), the beam will perform nearly like a pencil beam. The shadow radius and the radius of maximum transmittance mean that the laser beam will deviate from the required position. For a large Gaussian beam radius, there will actually be no shadow, but there is an evitable spreading that degrades the intensity of the laser beam.

On the other hand, we considered absorption of the vitreous body. For a pencil beam, the absorption is confined to the area near the point of incidence. For Gaussian beams, the absorption maximum goes deeper in the z direction and absorption shows a distribution in the radial direction. The absorption distribution is important for laser treatment. Absorption may result in changing the properties of the vitreous due to excessive heating, specially at the point of maximum heating.

Finally, it should be noted that Monte Carlo simulation provides the most accurate simulation of photon transport in turbid media, i.e., it is very efficient for our modeling purposes.

It should be stressed that there are many symptoms and vision problems associated with retinal hemorrhage that are considered more dangerous than that discussed for vitreous hemorrhage. For example, blood within the subretinal space may cause retinal damage by direct toxicity and through

physical separation of the neurosensory retina from the retinal pigment epithelium.

6 Conclusion

In this work, we studied light propagation in the vitreous humor contaminated by erythrocytes for the sake of analysis of the general case of vitreous hemorrhage.

We regarded the total medium, i.e., vitreous humor with erythrocytes, as a turbid medium. Then, we applied Monte Carlo simulation to obtain the total transmittance. Upon obtaining total transmittance, we are able to model the vision loss effects due to vitreous hemorrhage. This model revealed three parameters that characterize vision loss. The first parameter is the radius at which maximum transmission occurs. This parameter accounts for the position shift in viewing the pencil beam. The second parameter is the FWHM of the transmittance versus the radial distance profile. This parameter accounts for the effect that a very small size pencil beam upon emerging of the vitreous humor will appear as a circular bright strip of width equal to FWHM. This effect reduces the ability to differentiate two adjacent points in the viewed scene. The third parameter is the shadow radius, which accounts for a disk-shaped area extending from the projection of the pencil beam on the retina to the radial distance at which the transmittance is at the first half maximum. It is the dark area that occupies the area that was expected to be fully bright when there were no erythrocytes.

Through these three parameters, we are able to model vision loss effects due to vitreous hemorrhage. Moreover, these parameters have a strong effect on subsequent treatment using a laser beam to fix the cause of vitreous hemorrhage. The efficiency of the laser beam used in treatment will be greatly degraded due to the effects that result from scattering in the vitreous body.

Finally, we considered the absorption of the vitreous. We discussed total absorption and the absorption distribution. We demonstrate that excessive heating due to absorption may be dangerous, especially in the positions of maximum absorption. Correlations between the simulated results and parameters quantifying vision loss, such as visual acuity, visual SR, and contrast sensitivity have been discussed.

Future work may consider the aggregation of erythrocytes as they leak inside the vitreous humor, which is accounted for as a probability distribution of erythrocyte sizes. On the other hand, our analysis can be extended to imaging. In future work, we can study scattering effects on scans obtained by optical coherence tomography.

Acknowledgments

Constructive and critical comments made by the reviewers are acknowledged.

References

1. B. Hea, *Oftalmologia fundamentos*, Contexto, São Paulo (1991).
2. E. Ahmed, *A Textbook of Ophthalmology*, Phi Learning and Prentice Hall of India, India (2001).
3. P. H. Morse, A. Aminlari, and H. G. Scheie, "Spontaneous vitreous hemorrhage," *Arch. Ophthalmol.* **92**(4), 297–298 (1974).
4. R. W. Butner and A. R. McPherson, "Spontaneous vitreous hemorrhage," *Ann. Ophthalmol.* **14**(3), 268–270 (1982).
5. M. R. Dana et al., "Spontaneous and traumatic vitreous hemorrhage," *Ophthalmology* **100**(9), 1377–1383 (1993).
6. J. S. Lean and Z. Gregor, "The acute vitreous hemorrhage," *Br. J. Ophthalmol.* **64**, 469–471 (1980).
7. G. Lingren, L. Sjodell, and B. Lindblom, "A prospective study of dense spontaneous vitreous hemorrhage," *Am. J. Ophthalmol.* **119**(4), 458–465 (1995).
8. C. W. Spraul and H. E. Grossniklaus, "Vitreous hemorrhage," *Surv. Ophthalmol.* **42**(1), 3–39 (1997).
9. M. C. Ziemianski, J. W. Mc Meel, and E. P. Franks, "Natural history of vitreous hemorrhage in diabetic retinopathy," *Ophthalmology* **87**(4), 306–312 (1980).
10. M. Cordido et al., "Natural evolution of massive vitreous hemorrhage in diabetic retinopathy," *Retina* **8**(2), 96–101 (1988).
11. A. E. Kreiger and S. J. Haidt, "Vitreous hemorrhage in senile macular degeneration," *Retina* **3**(4), 318–321 (1983).
12. J. M. Googe et al., "Vitreous hemorrhage secondary to age-related macular degeneration," *Surv. Ophthalmol.* **32**(2), 123–130 (1987).
13. M. A. Tilanus et al., "Relationship between anticoagulant medication and massive intraocular hemorrhage in age-related macular degeneration," *Graefes Arch. Clin. Exp. Ophthalmol.* **238**(6), 482–485 (2000).
14. P. M. Tani, H. Buettner, and D. M. Robertson, "Massive vitreous hemorrhage and senile macular choroidal degeneration," *Am. J. Ophthalmol.* **90**(4), 525–533 (1980).
15. W. R. Lo et al., "Visual outcomes and incidence of recurrent vitreous hemorrhage after vitrectomy in diabetic eyes pretreated with bevacizumab (avastin)," *Retina* **29**(7), 926–931 (2009).
16. M. A. Novak et al., "Vitreous hemorrhage after vitrectomy for diabetic retinopathy," *Ophthalmology* **91**(12), 1485–1489 (1984).
17. F. I. Tolentino et al., "Vitreous hemorrhage after closed vitrectomy for proliferative diabetic retinopathy," *Ophthalmology* **96**(10), 1495–1500 (1989).
18. R. Rabinowitz et al., "Comparison between clinical and ultrasound findings in patients with vitreous hemorrhage," *Eye* **18**(3), 253–256 (2004).
19. M. S. Kocabora et al., "The predictive value of echography in diabetic vitreous hemorrhage," *Int. Ophthalmol.* **26**(6), 215–219 (2007).
20. A. N. Bashkatov et al., "Immersion clearing of human blood in the visible and near-infrared spectral regions," *Opt. Spectrosc.* **98**(4), 638–646 (2005); Translated from *Optika i Spektroskopiya* **98**(4), 695–703 (2005).
21. V. V. Tuchin, *Tissue Optics: Light Scattering Methods and Instruments for Medical Diagnosis*, 2nd ed., SPIE Press, Bellingham, Washington (2007).
22. C. F. Bohren and D. R. Huffman, *Absorption and Scattering of Light by Small Particles*, John Wiley & Sons Inc., New York (1983).
23. K. G. Kulikov and A. M. Radin, "Study of dispersion and absorption of an ensemble of spherical particles inside an optical cavity and new possibilities of predicting the optical characteristics of biological media by intracavity laser spectroscopy," *Opt. Spectrosc.* **92**(2), 199–206 (2002); Translated from *Optika i Spektroskopiya* **92**(2), 228–236 (2002).
24. K. G. Kulikov, "Light scattering by dielectric bodies of irregular shape in a layered medium in problems of biomedical optics: I. Theory and computational model," *Tech. Phys.* **57**(12), 1623–1631 (2012); From original Russian text: K. G. Kulikov, published in *Zhurnal Tekhnicheskoi Fiziki* **82**(12), 16–23 (2012).
25. A. Hoekstra, V. Maltsev, and G. Videen, *Optics of Biological Particles*, Springer, Dordrecht, The Netherlands (2007).
26. A. N. Korolevich, A. Y. Khairulina, and L. P. Shubochkin, "Scattering matrix of a monolayer of optically 'soft' particles at their dense package," *Opt. Spectrosc. (USSR)* **68**(2), 403–409 (1990).
27. A. N. Witt, "Multiple scattering in reflection nebulae. I. A Monte Carlo approach," *Astrophys. J.* **S35**, 1–6 (1977).
28. L. Wang, S. L. Jacques, and L. Zheng, "MCML-Monte Carlo modeling of light transport in multi-layered tissues," *Comput. Methods Programs Biomed.* **47**(2), 131–146 (1995).
29. D. K. Sardar et al., "Optical properties of ocular tissues in the near infrared region," *Lasers Med. Sci.* **22**(1), 46–52 (2007).
30. M. M. Kugeiko and S. A. Lisenko, "Determination of the spectral values of the real part of the relative refractive index of human blood erythrocytes from the measured directional scattering coefficients," *Opt. Spectrosc.* **105**(1), 147–153 (2008); From original Russian text: M. M. Kugeiko and S. A. Lisenko, published in *Optika i Spektroskopiya* **105**(1), 160–167 (2008).
31. M. M. Kugeiko and S. A. Lysenko, "Determination of the refractive index of spherical erythrocytes of human blood in the range 0.3–1.2 μm," *J. Appl. Spectrosc.* **74**(3), 425–429 (2007).

32. S. L. Jacques, C. A. Alter, and S. A. Prahl, "Angular dependence of HeNe laser light scattering by human dermis," *Lasers Life Sci.* **1**(4), 309–333 (1987).
33. L. Wang, S. L. Jacques, and L. Zheng, "CONV-convolution for responses to a finite diameter photon beam incident on multi-layered tissue," *Comput. Methods Programs Biomed.* **54**(3), 141–150 (1997).
34. S. K. Houston et al., "Lasers for the treatment of intraocular tumors," *Lasers Med. Sci.* **28**(3), 1025–1034 (2013).
35. R. L. Vincelette et al., "A comparison of a first-order thermal lensing model to a closed aperture Z-scan for the propagation of light in ocular media," *Proc. SPIE* **6084**, 60840G (2006).
36. W. Quan, G. Song, and Z.-Q. Wang, "An objective inspection method of visual acuity based on wave front aberrations of human eye," *Optik* **124**(12), 1320–1323 (2013).
37. J. D. Marsack et al., "Metrics of optical quality from wave aberrations predict visual performance," *J. Vis.* **4**(4), 322–328 (2004).
38. K. Zhang and D. Li, *Electromagnetic Theory for Microwaves and Optoelectronics*, 2nd ed., Springer-Verlag, Berlin, Heidelberg (2008).
39. D. G. Pelli and P. Bex, "Measuring contrast sensitivity," *Vis. Res.* **90**, 10–14 (2013).

Tarek A. Al-Saeed is an assistant professor at the Biomedical Engineering Department, Faculty of Engineering, Helwan University, Egypt. He received his BSc, MSc, and PhD degrees in electronics and communications engineering from Ain-Shams University, in 1994, 1999, and 2013, respectively. He received another PhD degree in biomedical engineering from Helwan University, in 2006. His current research interests include biomedical optics, optical biosensors, and image processing.

Sayed Y. El-Zaiat received his MSc and PhD degrees in optics at the Faculty of Science, University of Ain Shams, Cairo, Egypt, in 1986 and 1993, respectively. Currently, he is a professor of optics in Department of Physics, Faculty of Science, Ain Shams University. He is a member of Egyptian National Committee of Pure and Applied Physics. His research interests include optical interferometry, optical properties of materials, and multilayer thin films.